Soft Matter

Toughened Hydrogels Inspired by Aquatic Caddisworm Silk

Journal:	*Soft Matter*
Manuscript ID:	SM-ART-05-2015-001297.R1
Article Type:	Paper
Date Submitted by the Author:	20-Jul-2015
Complete List of Authors:	Stewart, Russell; University of Utah, Bioengineering Lane, Dwight; University of Utah, Bioengineering Weerasakare, G; University of Utah, Bioengineering Kaur, Sarbjit; University of Utah, Bioengineering

Toughened Hydrogels Inspired by Aquatic Caddisworm - Silk

Dwight D. Lane, Sarbjit Kaur, G. Mahika Weerasakare, and Russell J. Stewart*

Department of Bioengineering, University of Utah, Salt Lake City, UT 84112

* corresponding author

e-mail: russell.stewart@utah.edu

telephone: 801-581-8581

Abstract

Aquatic caddisworm silk is a tough adhesive fiber. Part of the toughening mechanism resides in serial, Ca^{2+}-phosphate crosslinked nano-domains that comprise H-fibroin, the major structural protein. To mimic the toughening mechanism, a synthetic phosphate-*graft*-methacrylate prepolymer, as a simple H-fibroin analog, was copolymerized within a covalent elastic network of polyacrylamide. Above a critical phosphate sidechain density, hydrogels equilibrated with Ca^{2+} or Zn^{2+} ions displayed greatly increased initial stiffness, strain-rate dependent yield behavior, and required 100 times more work to fracture than hydrogels equilibrated with Mg^{2+} or Na^{+} ions. Conceptually, the enhanced toughness is attributed to energy-dissipating, viscous unfolding of clustered phosphate-metal ion crosslinks at a critical stress. The toughness of the bioinspired hydrogels exceed the toughness of cartilage and meniscus suggesting potential application as prosthetic biomaterials. The tough hydrogels also provide a simplified model to test hypotheses about caddisworm silk architecture, phosphate metal ion interactions, and mechanochemical toughening mechanisms.

Introduction

Despite considerable progress in tissue engineering approaches to regenerate damaged or worn-out soft structural tissues, there likely will always be a need for inert, biocompatible, synthetic replacement materials.[1] Hydrogels of crosslinked water-soluble synthetic polymers have long been candidate materials for soft tissue prosthetics, partly because of their high water content and biocompatibility. Progress has been limited, though, because the structure and mechanical properties of conventional hydrogels have little resemblance to the exquisite hierarchical organization, strength, toughness, and graded mechanics of natural tissues. While the strength and stiffness of conventional hydrogels can be increased toward that of natural connective tissues by increasing the crosslink density, the resulting hydrogels are brittle and fracture at low strains. The usefulness of traditional synthetic hydrogels is also limited by their propensity to swell in watery environments, which further degrades their mechanical attributes.

New and creative approaches to synthesizing hydrogels have led to much tougher and fracture resistant materials more closely suited for soft structural tissue replacement.[2] Hydrogel toughness, as reflected in the work of extension to fracture, is a function of both stiffness and extensibility. A common architectural feature of the new generation of toughened hydrogels are two or more quasi-independent but interspersed networks, a stiffer network of energy-dissipating sacrificial linkages within a softer network of highly extensible linkages[3-5] Early double-network (DN) hydrogels comprised a densely crosslinked polymer network of 2-acrylamide-2-methylpropanesulfonic acid within a loosely crosslinked elastic polymer network of acrylamide.[6] The DN hydrogel possessed compressive strengths 20-40 times higher than

either hydrogel network alone. Because strain energy is dissipated by sacrificial chemical scission of polymer chains in the stiff network, permanent damage accumulates in the double covalent network hydrogels during strain cycles, resulting in poor fatigue resistance. Subsequent toughened DN hydrogel designs replaced the covalent sacrificial network with a network of reversible non-covalent sacrificial crosslinks. A multitude of non-covalent network linkages have been reported, including physical crosslinks,[7,8] hydrophobic bilayers,[9] dipole-dipole coupling,[10] electrostatic bonding between oppositely charged functional groups,[11] metal ion complexes,[12-14] and reversible polymer absorption to solid particles.[15,16] This latter group of DN hydrogels show, to varying extents, self-recovery of their initial dimensions and toughness during cyclical strains. Distinct from DN hydrogels, other reported approaches to toughening hydrogels include the use of multifunctional crosslinkers,[17] and hydrogels with uniform networks synthesized with symmetrical tetrahedral macromers.[18]

The adhesive silk of aquatic caddisworms is a tough natural multi-network fiber.[19,20] The silk is used by the larvae like a pressure-sensitive adhesive tape to bond gathered stones, sticks, or leaves into composite protective structures under water. Like natural tissues, the biphasic fibers contain around 70% water by mass. The initial modulus ranges from 80-140 MPa. The fibers yield at 2-5% strain, after which the stress plateaus, then gradually increases until the fibers fracture at an average stress over 30 MPa and strains of 100-150%. The yield stress shows a logarithmic strain-rate dependence, doubling over a two decade range of strain rates. The work of extension to fracture, around 17 MJ m^{-3}, is higher than the 7 MJ m^{-3} work of extension to fracture of the best reported synthetic DN hydrogels.[11] Caddisworm silk deformation is reversible; when strained to 20% then unloaded, the silk fibers recover 99% of

their initial dimensions, stiffness, and strength within 120 min. High strain cycle hysteresis and nearly full recovery allow the fibers to repeatedly dissipate energy to protect interfacial adhesive bonds, and thereby the structural integrity of the composite case. The tough, fatigue resistant, adhesive silk is highly adapted to the caddisworm's construction activities in an energetic aquatic niche. As such, it is an excellent natural source of design principles for development of tough synthetic materials for use in wet environments, including soft tissue prosthetics.

The viscoelasticity, toughness, and self-recovery of caddisworm silk has been attributed to a dynamic multi-network fiber structure.[20] We proposed a working model in which two independent metal ion-crosslinked protein networks each reversibly yield at different critical stress for a given strain rate.[20] Exchange of divalent metal ions in native fibers with monovalent Na^+ ions destroyed fiber stiffness, strength, yield behavior, and toughness.[19] In native fibers, Ca^{2+} is the predominant metal ion.[19,21] In our model, the first and stiffer metal ion-dependent network is crosslinked through Ca^{2+}-phosphoserine (pS) coordination complexes, the second softer network through Ca^{2+}-carboxylate complexes.[20] Our model includes a third, covalently crosslinked network, comprising in part a peripheral ring of peroxidase-catalyzed covalent dityrosine crosslinks,[22] which provides a passive elastic restoring force and memory of the permanent fiber structure to guide recovery of the metal ion-crosslinked yield domains when the fibers are unloaded. Although aquatic caddisworms (Trichoptera) are closely related phylogenetically to terrestrial silkworms (Lepidoptera), with numerous similarities apparent in their silk gland physiology and silk fiber molecular structure,[23,24] the silk toughening

mechanisms of caddisworm silk, based on multivalent metal ion coordination complexes, is more akin to other aquatic structural materials,[25] especially the byssal threads of mussels.[26-28]

The Ca^{2+}-phosphate crosslinks reside within and between H-fibroin proteins, by mass the major structural component of the silk fibers. H-fibroin is a large protein, M_m greater than 350,000 g/mol, with short and unique N- and C-termini flanking the central region, which comprises an imperfectly alternating pattern of three types of sequences blocks. Each type of repeating sequence contains at least one $(pSX)_n$ motif, wherein pS is phosphoserine, X is an aliphatic amino acid or arginine, and n=2-6.[21,29,30] In total, about 15 mol% of H-fibroin residues are pS, and on the order of 100 $(pSX)_n$ domains occur in each H-fibroin molecule.[20] The $(pSX)_n$ motifs have been predicted to form a serial arrangement of inter- and intrachain Ca^{2+}-stabilized β-domains,[19] on the order of 10 per H-fibroin, which are responsible for the initial stiffness and strength of the fibers, and the unfolding of which under strain is responsible for the distinct pseudo-yield point.[20] The Ca^{2+}-carboxylate crosslinks of the second dynamic network may occur within and between abundant PEVK-like structural proteins that have more than 20 mol% amino acids with carboxylate sidechains.[22]

The multi-network caddisworm silk model[20] relating silk molecular structure to fiber mechanics, and the natural toughening mechanism based on Ca^{2+}-phosphate coordination complexes, provided an initial framework for creating tough biomimetic hydrogels. Here, we report the synthesis of first generation multi-network hydrogels modeled after caddisworm silk with a first network crosslinked by reversible divalent metal ion-phosphate coordination complexes to provide strength, within a second covalently crosslinked elastic network of

polyacrylamide to provide extensibility and recovery from deformation. Mechanical characterization of the hydrogels demonstrated that their toughness, as reflected in work of extension to fracture, can exceed that of soft structural tissues, such as cartilage.

Materials and Methods

Materials. Phosphorus(V) oxychloride, 2-hydroxyethyl methacrylate, triethylamine, and glycidyl methacrylate were purchased from Alfa Aesar (Ward Hill, MA). 4-methoxyphenol was purchased from Tokyo Chemical Industry CO,. Ltd., (Tokyo, Japan). Methacrylic acid, 2,2'-azobis(2-methylpropionitrile), acrylamide, N,N'-methylene-bisacrylamide, and N,N,N',N'-tetramethylethylenediamine were purchased from Sigma Aldrich (St Louis, MO). Ammonium persulfate was purchased from Fischer Scientific (Pittsburgh, PA).

Phosphate monomer synthesis. 2-(methacryloyloxy)ethyl phosphate (MOEP) was synthesized as described previously.[31] Briefly, phosphorus oxychloride (33.9 g, 220 mmol) was mixed with hydroxyl-ethyl-methacrylamide (HEMA) at a 0.7:1 molar ratio in dry toluene (480 ml) under flowing argon. The reaction was stirred at 4°C while triethylamine (TEA) (77 ml) was added slowly over 10 min. Following addition of TEA, the reaction was stirred under argon gas for 6 hr at 22°C, then filtered to remove precipitated salt. The reaction was cooled to 4°C before addition of DI water (480 ml), then stirred under argon at 22°C for 2 hr. The reaction was extracted twice with diethyl ether (100ml). The organic layer was discarded. The aqueous layer was extracted using tetrahydrofuran (THF) and diethyl ether (1:2, 12 x 225ml), then dried over anhydrous sodium sulfate. The monomer was verified by ^{1}H and ^{31}P NMR.

Synthesis of polyMOEP-MA. PolyMOEP was synthesized by free radical polymerization of MOEP (85 mol%), and methacrylic acid (15 mol%) in methanol (12.5 ml/mg MOEP). The reaction was initiated with azo-bis-isobutyronitrile (AIBN, 4.5 mol%) at 55°C, and proceeded for 15 hr. The product was precipitated with acetone, then dissolved in water (200 ml H_2O per 17 g pMOEP). Subsequently, methacrylate groups (MA) were grafted onto the methacrylic acid sidechains with glycidyl methacrylate in 9-fold molar excess relative to the methacrylate sidechains. The methacrylated pMOEP (pMOEP-MA) was purified by tangential flow filtration using a Millipore Pellicon 3 cassette filter with an Ultracel 10 kD membrane. The polymer was washed with 10 volumes of water during filtration. The pH was adjusted to 7.3 with NaOH, the product lyophilized, and stored at -20° C. The resulting phosphate prepolymer contained 62.6 mol% phosphate sidechains, 10.9 mol% HEMA, and 26.5 mol% MA sidechains, as determined by ^{1}H and ^{31}P NMR. The molecular mass (M_m) and polydispersity index (PDI) of pMOEP-MA was determined by size exclusion chromatography (SEC) using an Amersham Pharmacia AKTA-FPLC system equipped with Wyatt MiniDawn Treos (light scattering) and Wyatt Optilab rEX (refractive index) detectors. The Superose 6 HR 10/30 column was equilibrated with 0.1 M sodium acetate (pH 6.5) containing 30% (vol/vol) acetonitrile. The average M_m and PDI were calculated using Wyatt MiniDawn ASTRA software to be 89 kg mol^{-1} and 2.6, respectively.

Hydrogel polymerization. Hydrogels were formed by free radical polymerization of acrylamide (Aam) and N,N'-Methylenebisacrylamide (Bis-Aam) with the pMOEP-MA prepolymer in 150 mM NaCl and 5 mM Tris (pH 8.0) (Fig. 1). The total wt% of Aam, Bis-Aam and MOEP-MA pre-polymer was held constant at 7.5%, while the wt% of the prepolymer was varied from 0.5% to 7.0 wt%. The molar ratio of Aam to Bis-Aam was 60:1. Polymerization was

initiated by adding 10% ammonium persulfate (APS) and tetramethylethylenediamine (TEMED) to final concentrations of 70 μg/ml and 2.4 μl/ml, respectively, to the monomer/pre-polymer solution. Polymerization proceeded in dog bone-shaped molds for 90 min at 22 °C. Molds were laser cut from 2 mm thick silicone rubber sheets, which were clamped between two acrylic plates to form the complete molds. A layer of mineral oil was floated on top of the polymerization reaction to limit exposure to oxygen. Polymerized gels were soaked in 150 mM NaCl, 5 mM Tris (pH 8) with repeated changes of solution for 24 hrs to remove unreacted materials.

Hydrogel metal ion exchange. Hydrogels were immersed in 150 mM NaCl, 10 mM tris (pH 8.0) with metal ions (Ca^{2+}, Mg^{2+}, or Zn^{2+}) added in 5 mM increments up to 50 mM over 24 hrs. Gradual addition of metal ions improved the homogeneity of the deswelled hydrogels. The hydrogels were then soaked in 50 mM metal ion and 10 mM Tris (pH 8.0) for an additional 24 hrs with frequent solution changes. Images of hydrogels were recorded using a dissection microscope during volume equilibration and their dimensions were measured using image J. Isotropic shrinking was assumed to calculate volume changes. Hydrogels were considered to be fully equilibrated when the volume reached steady state. Hydrogel density was measured by the buoyancy method using an analytical balance density kit (Mettler Toledo, Inc.) and calculated using the equation:

$$\rho_{sample} = \frac{(sample\ weight_{air}) * (\rho_{water} - \rho_{air})}{(sample\ weight_{air} - sample\ weight_{water})} + \rho_{air}$$

The density of water was corrected for temperature. Metal phosphate ratios were determined by ICP-OES of two independent hydrogel specimens at a commercial testing facility (Advanced Labs, Salt Lake City, UT).

Mechanical testing of hydrogels. Hydrogels were strained while submerged in 5 mM Tris, pH 8.0, containing 5 mM of the test metal ion on an Instron 3342 material test system controlled with Bluehill software (Instron, Inc.). Ca^{2+}-equilibrated hydrogels were strained at rates ranging from 0.01 to 1.0 s^{-1}. Strain to fracture and cyclical strain tests were done at 0.15 s^{-1}.

Infrared spectroscopy. Sodium equilibrated hydrogels were incubated overnight in 10 mM Na^+ EDTA to remove rouge divalent metal ions potentially scavenged during polymerization and processing. Na^+ gels were stored in 1 mM EDTA to prevent binding of trace divalent metal ions. Divalent metal ion hydrogels were equilibrated with the respective metal ion as described above. After volume equilibration, the samples were rinsed with water, then lyophilized to remove water, and crushed into a powder using an agar mortar and pestle before applying to the diamond ATR crystal. The IR spectra were normalized to the intensity of an absorption band centered at 1665 cm^{-1}, which corresponds to absorption by amide groups in the polymethacrylamide backbone.[43] A linear baseline correction was applied to the intensity normalized spectra between 800 and 1300 cm^{-1}, which contains several phosphate vibrational modes. ATR-FTIR absorbance spectra were collected using a Nicolet 6700 spectrometer (Thermo Scientific, FL) with a diamond Smart iTR accessory, a deuterated triglycine sulfate detector, and a KBr/Ge mid-infrared optimized beamsplitter. Spectra were recorded with a resolution of 4 cm^{-1} and as 512 averaged scans.

Processing of experimental data. Data was processed in matlab (MathWorks). Linear fits to the initial part of the stress strain curve were used to estimate the initial modulus. The yield point was determined using a 5% strain offset from the initial linear portion of the curve. Energy dissipation, strain cycle hysteresis, was computed by subtracting the trapezoidal integration of the reverse curve from the forward curve of cyclical tests. Residual strain was measured by extending the initial linear portion of the stress strain curve (disregarding toe regions) through the base line.

Results

Synthesis of divalent metal-ion crosslinked double network hydrogels. The toughness of natural caddisfly silk is contributed mostly by the Ca^{2+}-phosphate crosslinked $(pSX)_n$ domains in the H-fibroin protein.[20] To create a simple analog of H-fibroin, polymethacrylate random copolymers were synthesized with varying mol% of ethyl-phosphate (MOEP), ethyl-hydroxy (HEMA) sidechains, and carboxylate (MAA) sidechains (Fig. 1A). The MAA groups were subsequently grafted with glycidyl methacrylate as crosslinking groups. To prepare double network hydrogels, the mono-sodium salt of methacrylated polyphosphate (pMOEP-MA) prepolymers were mixed with acrylamide (AAM) and bisacrylamide (Bis-AAM) monomers and copolymerized in 150 mM NaCl, and 5 mM Tris (pH 8.0). The total wt% of polymer in the hydrogels was kept constant at 7.5 wt%. During polymerization, the pMOEP-MA prepolymer became crosslinked into the pAAM network through the MA sidechains (Fig. 1B). The pAAM network served as an analog of the passive elastic network of natural caddisfly silk. The resulting dog bone-shaped hydrogels, with Na^+ counterions, were clear and transparent.

As Na^+ was exchanged with the divalent metal-ions, Mg^{2+}, Ca^{2+}, and Zn^{2+}, the hydrogels shrank to about 65% of their initial volume (Table 1). The final volume had little dependence on the divalent metal ion species (Fig. 2). However, the hydrogels shrank fastest in Mg^{2+}, equilibrating in 90 min, whereas volume equilibration in both Ca^{2+} and Zn^{2+} took approximately 24 hrs. During divalent metal ion exchange, the initially transparent Na^+-hydrogels became slightly translucent. The resulting divalent ion-equilibrated DN hydrogels had three types of crosslinks within and between networks: covalent Bis-AAM junctions between pAAM chains, covalent Bis-AAM junctions between pAAM and methacrylated side chains in pMOEP networks, and reversible phosphate/metal ion junctions within the pMOEP network, which were likely a mix of inter- and intramolecular crosslinks (Fig 1C).

The mechanical effect of varying the ratio of the pMOEP-MA prepolymer network to the pAAM network in hydrogels equilibrated with Ca^{2+} ions was evaluated by tensile testing. The concentration of pMOEP-MA prepolymer was varied from 1.5 to 7.0 wt% while holding the total polymer/monomer concentration constant at 7.5 wt% (Fig. 3A). The hydrogels were strained to failure at room temperature (20-22°C) while fully submerged in a water bath to prevent water evaporation and to limit potential effects of uneven water flux out of and into the gels. The bath solutions contained 5 mM Ca^{2+} and were buffered at pH 8.0, above the pK_{a2} of the phosphate sidechains. At the lowest ratio of pMOEP-MA to pAAM, 1.5:6.0 wt%, the Ca^{2+}-equilibrated hydrogels were soft with an initial modulus of 0.020 +/- 0.004 MPa. The stress increased linearly with strain until fracture occurred at 0.054 +/- 0.002 MPa and less than 150% strain (Fig. 3A). As the pMOEP-MA to pAAM ratio was increased to above 5 wt% pMOEP-MA, the initial modulus rose sharply, strain at fracture increased toward 200%, and yield-like

behavior—dramatic strain softening—appeared around 20% elongation (Fig 3A). Hydrogel toughness, as reflected in the work of extension to fracture (Fig. 3B), also increased sharply with increasing pMOEP-MA, due primarily to the increase in yield stress of the hydrogels.

Hydrogel synthesis using pMOEP-MA as a prepolymer with a high mol% of phosphate sidechains was essential to toughen the Ca^{2+}-crosslinked DN hydrogels. Other hydrogel synthesis methods failed to produce toughened hydrogels. For example, hydrogels of 7.5 wt% pMOEP-MA with no pAAM, were brittle and frequently fractured during equilibration with divalent metal ions. Hydrogels prepared with 6.5 mol% pMOEP-MA with only 40 mol% phosphate sidechains stiffened considerably with Ca^{2+}, but did not display yield-like behavior, shrank less during equilibration with Ca^{2+}, and were less tough (not shown). Hence, further DN hydrogel mechanical characterization was done with hydrogels synthesized with 6.5 wt% pMOEP-MA and 1.0 wt% pAAM/Bis-AAM.

Hysteresis and self-recovery kinetics of Ca^{2+}-crosslinked hydrogels during cyclical loading. The yield-like response of Ca^{2+} hydrogels was not a permanent plastic deformation. Instead, the initial length, modulus, and yield stress of hydrogels strained to 50% recover approximately 90% of their initial values within 90 mins after unloading (Fig. 5 and 6). Hence, we refer to the phenomenon as pseudo-yield. The area within the forward and reverse curves of the highly hysteretic cycles represents dissipated strain energy, which also recovered to approximately 90% of the initial cycle value within 90 mins. The recovery did not fit a single exponential process. In contrast, Mg^{2+} hydrogels had a linear elastic response to cyclical strains, displaying little hysteresis (Fig. 5A, green curves). Hydrogels equilibrated with Zn^{2+} were more

brittle beyond the pseudo-yield point and could not be reliably strained to 50% elongation. Therefore the rate of refolding was not determined.

Strain Rate Dependence of Ca^{2+}-crosslinked hydrogels. The pseudo-yield stress of Ca^{2+}-equilibrated hydrogels strained to 100% at strain rates ranging over three orders of magnitude increased 5-fold (Fig. 6B). Likewise, the initial modulus, work of extension, and dissipated energy increased by, 60%, 2-fold, and 2.3-fold, respectively (not shown). Pseudo-yield stress had a logarithmic dependence on strain rate (Fig. 6B). Strain rate had little effect on residual strain, which varied by only 5% over the range of strain rates.

Metal ion species dependence of hydrogel toughness. Hydrogels containing Na^+ counter ions were soft, linear elastomers that could be elongated about 250% before fracture (Fig. 4 and Table 1). Exchange with divalent metal ions increased the pseudo-yield stress in the following order: $Mg^{2+} < Ca^{2+} < Zn^{2+}$. Hydrogels exchanged with Mg^{2+}, like Na^+ hydrogels, were soft and displayed a linear dependence of stress on strain, whereas Ca^{2+} and Zn^{2+} hydrogels both displayed dramatic strain softening (yield-like) behavior around 20% strain. Although Zn^{2+} hydrogels fractured soon after the yield point, at strains of 40% compared to average strains of 90% for Ca^{2+} hydrogels, the work to fracture of Ca^{2+} and Zn^{2+} was nearly the same, 10.4 and 10.5 MJ m^{-3}, respectively, more than three times higher than Mg^{2+} (Table 1).

IR spectroscopy of divalent metal-ion crosslinked hydrogels. Interactions of divalent metal ions with phosphate sidechains was evaluated by IR spectroscopy (Fig. 8). Bands corresponding to degenerate $P\text{-}O^-$ symmetric stretching modes occur between 950 and 1050 cm^{-1}. Band assignments were based on literature precedents for primary phosphate esters and pH titrations.[20,32,33] The Na^+ absorption band centered at 962 cm^{-1} corresponds to the combined

absorption of two identical P-O^- bonds of dibasic phosphate. The 962 cm^{-1} band appears to split when divalent metal ions are added, possibly because the bonds are not identical in the divalent metal ion complexes. Similar splitting and shifting of this phosphate band has been observed in caddisworm silk equilibrated with Na^+ vs. divalent metal ions.[20] The split band was blue-shifted 40 cm^{-1} for both Mg^{2+} and Zn^{2+}, and 30 cm^{-1} for Ca^{2+}. The absorbance intensity of the shifted band increased in the order: $Zn^{2+} > Ca^{2+} > Mg^{2+}$.

Discussion

Caddisworm-inspired hydrogel structure and mechanics. Above a threshold density of phosphate sidechains on the pMOEP prepolymer, exchange of monovalent Na^+ with divalent metal ions resulted in collapse of the DN hydrogel structure, accompanied by exclusion of about 40% of its equilibrium water mass (Table 1), and a change in appearance from transparent to slightly translucent. Mechanically, the hydrogels transitioned from soft and elastic to tough and viscoelastic with non-permanent strain softening (yield) at a critical stress (Fig. 7). The synthetic method of concentrating the phosphate groups on a prepolymer as a separate, but covalently connected network within a second polyacrylamide network was critical to achieve the viscoelastic behavior and toughening effect on the hydrogels.

We interpret these observations as evidence divalent cations crosslinked the polyphosphate prepolymer network, both intra- and intermolecularly, through the phosphate sidechains into dense partially dehydrated clusters, as illustrated in figure 2C, that function as pseudo-domains. The collapsed phosphate prepolymer clusters are connected to one another through the elastic polyacrylamide network. The toughening effect—the extra work required to fracture the Ca^{2+} equilibrated hydrogels versus the Na^+ equilibrated hydrogels—was due to

energy absorbed and dissipated by rupture and unfolding of the Ca^{2+} phosphate crosslinked clusters. The dense clusters functioned as a series of sacrificial yield domains undergoing sequential, viscous unfolding and extension in the stress plateau region. Rupture of the Ca^{2+} phosphate crosslinked clusters was reversible, which allowed the domain-like regions to slowly reform when unloaded, guided by the memory of the elastic polyacrylamide network. About 90% of the capacity to dissipate strain energy at moderate strain rates was recovered within 90 min. The less than complete recovery suggested some permanent damage occurred during the first strain cycle. The fatigue resistance of the hydrogels has yet to be thoroughly characterized.

Modulating hydrogel strength and toughness with divalent metal ions. The stress response of the caddis silk-mimetic hydrogels can be tuned to some extent by multivalent metal ion selection, as one means to design hydrogels to meet the specifications of a particular application. Details of the metal ion interactions with the phosphate sidechains are not known, but several observations are worth noting. According to the HSAB classification scheme, Mg^{2+} and Ca^{2+} are hard acids, Zn^{2+} is intermediate, and dibasic phosphate is a hard base.[34] The interaction between non-polarizable hard acids and hard bases is predominantly ionic in character. Therefore, the divalent metal ion-phosphate complexes in the DN hydrogels may be more electrostatic in character, as opposed to charge transfer complexes. Exchange of Na^{+} with Mg^{2+} caused dehydration and deswelling of the hydrogels to similar extents as Ca^{2+} and Zn^{2+}, although deswelling was fastest in Mg^{2+} (Fig. 2). The interaction of Mg^{2+} with phosphate sidechains was likewise evident in the blue-shift of absorption bands corresponding to the $P\text{-}O^{-}$ symmetric stretching modes in the IR spectra (Fig. 8). Despite evidence of phosphate Mg^{2+}

coordination complexes, the complexes did not function as load bearing crosslinks in the hydrogels since there was comparatively little stiffening of the Mg^{2+} equilibrated hydrogels compared to Ca^{2+} and Zn^{2+} hydrogels (Fig. 7). Significantly, the weak mechanical effect of Mg^{2+} phosphate complexation, despite similar dehydration and volume change, rules out that the increased stiffness, strength, pseudo-plastic yield, viscoelasticity, and hysteresis of hydrogels equilibrated with Ca^{2+} and Zn^{2+} was due to more extensive dehydration and deswelling.

The preferred coordination geometry of Mg^{2+} is octahedral both in water and when bound by proteins or nucleic acids. In water, the coordination geometry is satisfied with six inner sphere water molecule ligands. Perturbing this rigid coordination geometry is energetically costly.[35] Proteins and nucleic acids bind Mg^{2+} ions differently; protein sidechain ligands bind Mg^{2+} directly (inner sphere mode), while nucleic acids bind Mg^{2+} indirectly through the hydration shell (outer sphere mode). Protein Mg^{2+} binding sites are usually buried in the protein interior where the low dielectric constant makes ligand exchange between inner sphere waters and anionic sidechains more energetically favorable.[36] All protein Mg^{2+}-binding sites retain at least one, and on average 2.2 inner sphere H_2O molecules in the Mg^{2+} binding site.[37] In nucleic acids, on the other hand, Mg^{2+} ions are usually complexed by outer sphere phosphate oxygens leaving the octahedral hydration shell intact, or mostly intact.[38] For example, of the four octahedral Mg^{2+} ions that stabilize tRNA tertiary structure, one is bound as $Mg(H_2O)_6^{2+}$, two as $Mg(H_2O)_5^{2+}$, and one as $Mg(H_2O)_4^{2+}$, with zero, one, and two direct inner sphere phosphate oxygen coordinate bonds, respectively.[39] The weak effect of Mg^{2+} on pMOEP/pAMM hydrogel mechanics may be due to indirect coordination of $Mg(H_2O)_6^{2+}$ ions as outer sphere ligands by phosphate sidechains, or as a mix of outer and inner shell ligands with

only partial exchange of inner shell water molecules, as observed in tRNAs. Although the blue shift of the P-O^- symmetric stretching mode band suggests at least some direct inner sphere coordination between Mg^{2+} and phosphates, the predominantly outer sphere nature of the phosphate-Mg^{2+} complexes may be too weak or too dynamic to form load bearing intra- or inter-chain crosslinks.

The greater stiffness and strength of the Ca^{2+} and Zn^{2+} hydrogels may be due to a greater propensity for their hydration shells to be displaced by inner sphere phosphate oxygen bonds, which may result in effectively stronger, load bearing, inter- and intra-chain crosslinks. The coordination numbers and geometries of Ca^{2+} and Zn^{2+} are more flexible than Mg^{2+}, and there are smaller energy barriers for transitions between coordination number and geometry.[37] In protein binding sites, Ca^{2+} ions mostly have 6 or 7 inner sphere oxygen ligands, and on average only 1.5 H_2O ligands.[40] Protein bound Zn^{2+} ions have a coordination number of six when coordinated by oxygen ligands, as is the case in the pMOEP/pAAM hydrogels. The radii, 0.74-1.04 Å and 0.71-1.03 Å, respectively, and therefore charge densities of Zn^{2+} and Mg^{2+} ions are similar.[44] The higher charge densities of Zn^{2+} and Mg^{2+} produce a blue shift of similar magnitude, 40 cm^{-1} relative to Na^+, in the P-O^- symmetric stretching mode (Fig. 8). Divalent Ca^{2+} ions, which have a radius of 1.14-1.48 Å and lower charge density than Zn^{2+} and Mg^{2+}, produce a smaller blue shift of 30 cm^{-1} relative to Na^+ ions. Although their respective absorption coefficients are not known, the higher absorption intensity in the Zn^{2+} band compared to Mg^{2+} may be evidence that Zn^{2+} forms more inner sphere bonds with phosphate oxygens than Mg^{2+}, which may account for its much greater effect on hydrogel mechanical properties. The higher strength and stiffness of Zn^{2+} hydrogels compared to Ca^{2+} hydrogels may be due to stronger

phosphate crosslinks, which in turn may be due to higher coordinate bond strengths, or the geometry of the complexes, or the number of complexes. The contribution, if any, of the higher Zn to P ratio compared to Ca and Mg is unknown and requires further investigation. The similar work of extension to failure, or toughness, of the Ca^{2+} and Zn^{2+} hydrogels is difficult to explain and may be coincidental.

Comparisons to other DN hydrogels, natural and synthetic. Several aspects of the mechanical response of natural silk fibers to controlled strains, including pseudo-yield behavior, logarithmic strain rate dependence, and self-recovery,[20] were qualitatively reproduced in the caddisworm silk mimetic DN hydrogels. The initial stiffness and work of extension to failure (toughness) fell well short of the natural fibers (Table 1, Fig. 9k). Much of the toughness of natural caddisfly silk is due to strain stiffening beyond the stress plateau region, where presumably the viscoelastic yield domains have been mostly unfolded.[19] In future work, design efforts will be directed, in part, toward increasing the stiffness and strength of the elastic network to further improve toughness of the synthetic DN hydrogels. The hydrogel toughening effect required high concentrations of phosphate sidechains compared to the natural fibers. The greater stiffness, yield stress, and fatigue resistance of the natural fibers with lower densities of Ca^{2+}-phosphate crossbridges may result from greater cooperativity in the strain dependent unfolding and refolding of the highly organized Ca^{2+}-phosphate β-domains compared to the random, less organized Ca^{2+}-phosphate pseudo-domains in the synthetic hydrogels.[20,21,41] Another factor may be the effective dielectric constant in the vicinity of the metal ion-phosphate bonds. The precise folding of β-domains in the natural fibers may exclude water from the local environment of the Ca^{2+}-phosphate complexes more effectively than the

random collapse of the polyphosphate chains in the hydrogels. If so, the dielectric constant would be lower and the strength of the Ca^{2+} ion-phosphate bonds higher in the natural fibers than in the hydrogels.

The strength and toughness of the first generation caddisworm silk inspired hydrogels compare favorably with other reported synthetic DN hydrogels (Fig. 9). The initial modulus of Ca^{2+} hydrogels was in the same range as previous DN hydrogels, while Zn^{2+} hydrogels were considerably stiffer. Both Ca^{2+} and Zn^{2+} hydrogels were tougher than all other synthetic DN hydrogels, primarily because of greater stiffness rather than extreme extensibility. Synthetic hydrogels that achieve high toughness primarily through being highly extensible are not suitable as mechanical replacements for soft structural tissues, which do not operate under such extreme strains. Over three decades of strain rate, the initial stiffness and yield stress increased five-fold for the Ca^{2+} equilibrated pMOEP/pAAM hydrogels, and strain cycle energy dissipation (hysteresis) more than doubled (Fig. 6). Comparison of strain rate dependence of caddis silk-inspired DN hydrogels to earlier DN hydrogel architectures is difficult because strain rate dependence has rarely been reported. Strain rate dependence is a critical feature of viscoelastic hydrogels because the utility of a material will be limited to applications were the mechanical response is appropriate for the expected strain rates. At very low strain rates, below the relaxation time of the viscous yield domains, the toughening mechanism becomes irrelevant; the stress response of the hydrogels will correspond to only the elastic network component. Under sudden sustained loads, the stress will relax to the load supported by extension of the elastic network only. Finally, the mimetic hydrogels are tougher than articular cartilage and the fibrocartilage meniscus when compared to reported values of tissues that

were loaded in tension (Fig. 9i,j).[42] The materials were compared in tension because cartilage and menisci loaded in unconfined compression experience radial tensile forces.

Conclusions. Using a greatly simplified polyphosphate analog of H-fibroin as a prepolymer network with dynamic phosphate metal ion crosslinks within an extensible polyacrylamide network a DN network hydrogel architecture was created that qualitatively replicated the mechanical properties of natural caddisworm silk, including high stiffness, pseudo-yield behavior, logarithmic strain rate dependence, high strain cycle hysteresis, and self-recovery. It was possible to replicate the mechanical properties by copying only relatively simple and synthetically accessible structural features of the natural fiber. We are confident that as further details of the natural caddisworm silk fiber architecture and metal phosphate chemistry are determined, the design of synthetic hydrogels can be improved to bring their toughness closer to the natural fibers. Beyond their potential utility as prosthetic biomaterials, the caddisworm mimetic hydrogels provide a simplified, inexpensive, and convenient model system to test hypotheses concerning the relationship between chemistry, structure, and mechanical properties of natural silk fibers.

Acknowledgements

This work was supported by the Army Research Office, award #W911NF1310319. We thank Nic Ashton for helpful discussions and Monika Sima for help with SEC.

References

(1) Vrancken, A. C. T.; Buma, P.; van Tienen, T. G. *Int. Orthop.* **2012**, *37*, 291–299.
(2) Haque, M. A.; Kurokawa, T.; Gong, J. P. *Polymer* **2012**, *53*, 1805–1822.
(3) Naficy, S.; Brown, H. R.; Razal, J. M.; Spinks, G. M.; Whitten, P. G. *Aust. J. Chem.* **2011**, *64*, 1007.
(4) Zhao, X. *Soft Matter* **2014**, *10*, 672–687.
(5) Long, R.; Mayumi, K.; Creton, C.; Narita, T.; Hui, C.-Y. *Macromolecules* **2014**, *47*, 7243–7250.
(6) Gong, J. P.; Katsuyama, Y.; Kurokawa, T.; Osada, Y. *Adv. Mater.* **2003**, *15*, 1155–1158.
(7) Chen, Q.; Zhu, L.; Zhao, C.; Wang, Q.; Zheng, J. *Adv. Mater.* **2013**, *25*, 4171–4176.
(8) Myung, D.; Koh, W.; Ko, J.; Hu, Y.; Carrasco, M.; Noolandi, J.; Ta, C. N.; Frank, C. W. *Polymer* **2007**, *48*, 5376–5387.
(9) Haque, M. A.; Kurokawa, T.; Kamita, G.; Gong, J. P. *Macromolecules* **2011**, *44*, 8916–8924.
(10) Han, Y.; Bai, T.; Liu, Y.; Zhai, X.; Liu, W. *Macromol. Rapid Commun.* **2011**, *33*, 225–231.
(11) Sun, T. L.; Kurokawa, T.; Kuroda, S.; Bin Ihsan, A.; Akasaki, T.; Sato, K.; Haque, M. A.; Nakajima, T.; Gong, J. P. *Nat. Mat.* **2013**, *12*, 932–937.
(12) Kersey, F. R.; Loveless, D. M.; Craig, S. L. *J R Soc Interface* **2006**, *4*, 373–380.
(13) Henderson, K. J.; Zhou, T. C.; Otim, K. J.; Shull, K. R. *Macromolecules* **2010**, *43*, 6193–6201.
(14) Sun, J.-Y.; Zhao, X.; Illeperuma, W. R. K.; Chaudhuri, O.; Oh, K. H.; Mooney, D. J.; Vlassak, J. J.; Suo, Z. *Nature* **2012**, *489*, 133–136.
(15) Lin, W.-C.; Fan, W.; Marcellan, A.; Hourdet, D.; Creton, C. *Macromolecules* **2010**, *43*, 2554–2563.
(16) Rose, S.; Dizeux, A.; Narita, T.; Hourdet, D.; Marcellan, A. *Macromolecules* **2013**, *46*, 4095–4104.
(17) Qin, X.; Zhao, F.; Liu, Y.; Wang, H.; Feng, S. *Colloid Polym Sci* **2009**, *287*, 621–625.
(18) Sakai, T.; Matsunaga, T.; Yamamoto, Y.; Ito, C.; Yoshida, R.; Suzuki, S.; Sasaki, N.; Shibayama, M.; Chung, U.-I. *Macromolecules* **2008**, *41*, 5379–5384.
(19) Ashton, N. N.; Roe, D. R.; Weiss, R. B.; Cheatham, T. E.; Stewart, R. J. *Biomacromolecules* **2013**, *14*, 3668–3681.
(20) Ashton, N. N.; Stewart, R. J. *Soft Matter* **2015**, *11*, 1667–1676.
(21) Stewart, R.; Wang, C. *Biomacromolecules* **2010**, *11*, 969–974.
(22) Wang, C.-S.; Ashton, N. N.; Weiss, R. B.; Stewart, R. J. *Insect Biochem. Mol. Biol.* **2014**, *54*, 69–79.
(23) Yonemura, N.; Mita, K.; Tamura, T.; Sehnal, F. *J. Mol. Evol.* **2009**, *68*, 641–653.
(24) Sehnal, F.; Zurovec, M. *Biomacromolecules* **2004**, *5*, 666–674.
(25) Degtyar, E.; Harrington, M. J.; Politi, Y.; Fratzl, P. *Angew. Chem. Int. Ed.* **2014**, *53*, 12026–12044.
(26) Harrington, M. J.; Waite, J. H. *J. Exp. Biol.* **2007**, *210*, 4307–4318.
(27) Harrington, M.; Masic, A.; Holten-Andersen, N.; Waite, J.; Fratzl, P. *Science* **2010**, *328*, 216.
(28) Holten-Andersen, N.; Jaishankar, A.; Harrington, M. J.; Fullenkamp, D. E.; DiMarco, G.; He, L.; McKinley, G. H.; Messersmith, P. B.; Lee, K. Y. C. *J. Mater. Chem. B* **2014**, *2*, 2467–2472.
(29) Yonemura, N.; Sehnal, F.; Mita, K.; Tamura, T. *Biomacromolecules* **2006**, *7*, 3370–3378.
(30) Ohkawa, K.; Miura, Y.; Nomura, T.; Arai, R.; Abe, K.; Tsukada, M.; Hirabayashi, K. *Biofouling* **2013**, *29*, 357–367.
(31) Shao, H.; Weerasekare, G. M.; Stewart, R. J. *J. Biomed. Mater. Res.* **2011**, *97A*, 46–51.
(32) Sanchez-Ruiz, J.; Martinez-Carrion, M. *Biochemistry* **1988**, *27*, 3338–3342.
(33) Fernández, C.; Ausar, S. F.; Badini, R. G.; Castagna, L. F.; Bianco, I. D.; Beltramo, D. M. *Int. Dairy Journal* **2003**, *13*, 897–901.
(34) Pearson, R. G. *J. Am. Chem. Soc.* **1963**, *85*, 3533–3539.
(35) Bock, C. W.; Kaufman, A.; Glusker, J. P. *Inorg. Chem.* **1994**.
(36) Dudev, T.; Lim, C. *Chemical Reviews* **2003**, *103*, 773–788.

(37) Katz, A. K.; Glusker, J. P.; Beebe, S. A. *J. Am. Chem. Soc.* **1996**, *118*, 5752–5763.
(38) Robinson, H.; Gao, Y. G.; Sanishvili, R.; Joachimiak, A.; Wang, A. H. *Nucleic Acids Res.* **2000**, *28*, 1760–1766.
(39) Holbrook, S. R.; Sussman, J. L.; Warrant, R. W.; Church, G. M.; Kim, S.-H. *Nucleic Acids Res.* **1977**, *4*, 2811–2820.
(40) Glusker. **2000**, 1–10.
(41) Keten, S.; Xu, Z.; Ihle, B.; Buehler, M. J. *Nat. Mater.* **2010**, *9*, 359–367.
(42) Danso, E. K.; Honkanen, J. T. J.; Saarakkala, S.; Korhonen, R. K. *J. of Biomechanics* **2014**, *47*, 200–206.
(43) Stuart, B. *Infrared Spectroscopy: Fundamentals and Applications*. **2004**, John Wiley & Sons, Hoboken, NJ
(44) Cotton, F.A.; Wilkinson, G.; Murillo, C.A.; Bochmann, M. *Advanced Inorganic Chemistry*, 6th Ed., **1999**, John Wiley & Sons, New York, NY

1

Table 1. Composition and properties of DN hydrogels and native caddisworm silk

	pMOEP/pAAm Hydrogels*				Native caddisworm silk[§]
Ion:	Zn^{2+}	Ca^{2+}	Mg^{2+}	Na^{+}	$(Ca^{2+})^{\#}$
Volume (% of initial)	66.2 ± 1.2	66.5 ± 2.1	63.6 ± 3.3	97.2 ± 2.4	--
Water (wt %)	53.6 ± 1.3	55.6 ± 2.1	56.3 ± 1.9	92.5 ± 0.5	66**
Density (g/cm^3)	1.10 ± 0.02	1.07 ± 0.02	1.05 ± 0.02	1.01 ± 0.01	--
M/P molar ratio	3.9	1.7	1.5	--	--
Initial Modulus (MPa)	34.2 ± 2.5	10.3 ± 3.5	0.1 ± 0.04	0.04 ± 0.01	86.5 ± 19.2
Yield Stress (MPa)	3.5 ± 0.4	1.8 ± 0.2	No Yield	No Yield	2.8 ± 0.4
Stress at Fracture (MPa)	3.8 ± 0.3	1.9 ± 0.1	0.3 ± 0.01	0.05 ± 0.004	32.7 ± 6.6
Elongation at Fracture (%)	40 ± 10	90 ± 50	220 ± 20	227 ± 14	126 ± 29
Work to Fracture (MJ/m^3)	10.4 ± 0.4	10.5 ± 1.2	0.3 ± 0.004	0.09 ± 0.01	17.3 ± 6.2

*6.5 wt% pMOEP, 1.0 wt% pAAM, [§]mechanical data from refs. 16 and 17. [#]Native caddisworm silk contains mostly Ca^{2+}. **unpublished

Figures:

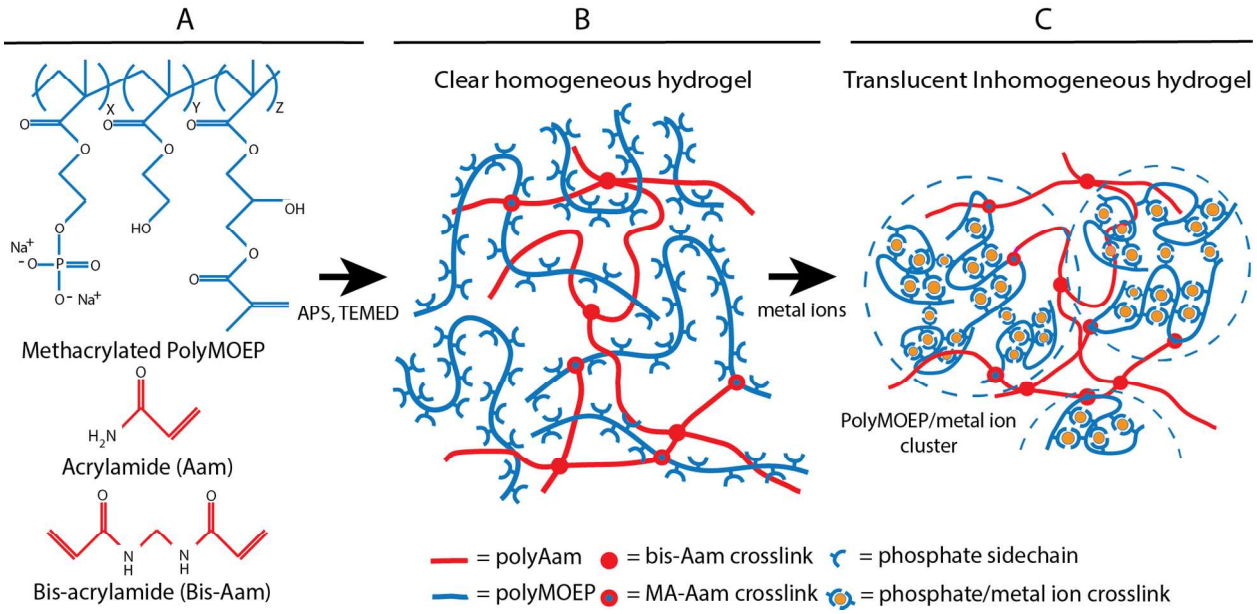

Figure 1. Double network hydrogel synthesis. A.) The sodium salt of the pMOEP prepolymer was copolymerized with AAm and Bis-AAm monomers. The total polymer concentration was kept constant at 7.5 wt%. B.) The pAAm network was covalently connected to the pMOEP network through MA sidechains to form a double network hydrogel. C.) The pMOEP network was crosslinked and de-swelled by exchange of Na^{+} with divalent metal ions (Mg^{2+}, Ca^{2+}, and Zn^{2+}). The collapsed pMOEP-divalent metal ion network is conceptualized as dense clusters that function as sacrificial yield domains.

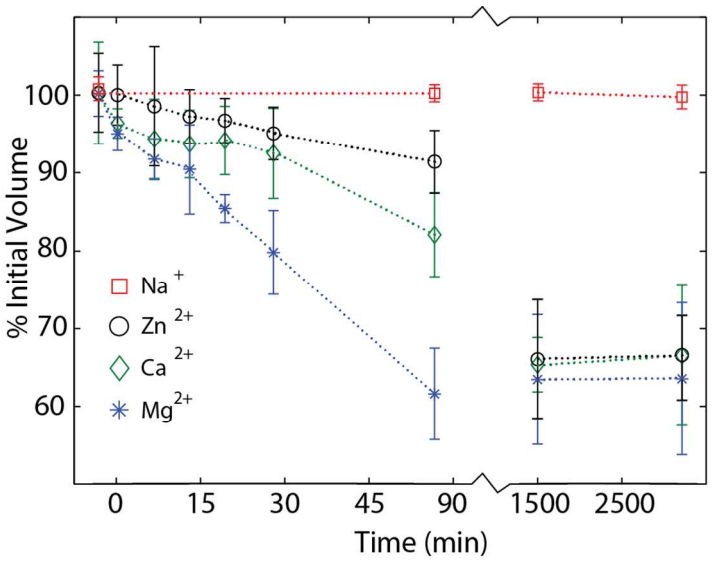

Figure 2. Hydrogel volume change during metal ion exchange. The hydrogels contained 7.5 total wt% polymer, comprising 6.5 wt% pMOEP and 1.0 wt% pAAm, before deswelling by the addition of divalent metal ions. For each data point n=3 and error bars = ± 1 s.d..

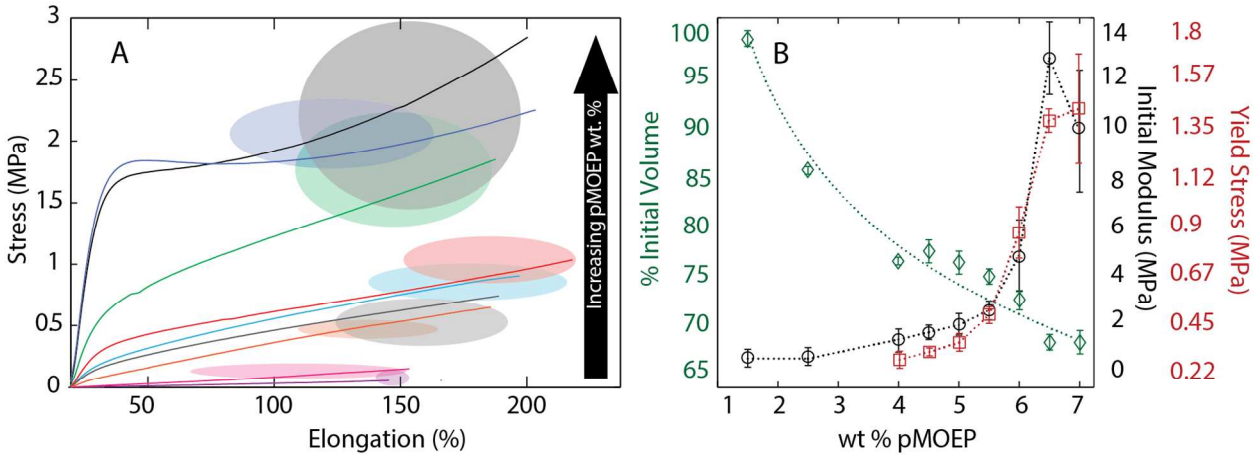

Figure 3. Critical pMOEP concentration dependence of Ca^{2+}-hydrogel toughening. A.) Representative stress strain curves for hydrogels prepared with increasing pMOEP and decreasing pAAm concentrations. The total polymer wt% was fixed at 7.5 wt%. Ovals represent the area enclosed by ± 1 s.d. of the mean stress and elongation for each hydrogel formulation (n ≥ 3). B.) The equilibrium volume of the hydrogels declined with increasing pMOEP/pAAm wt% ratio. The initial modulus and yield stress had a non-linear dependence on pMOEP/pAAm wt% ratio. Error bars represent ± 1 s.d., n ≥ 3.

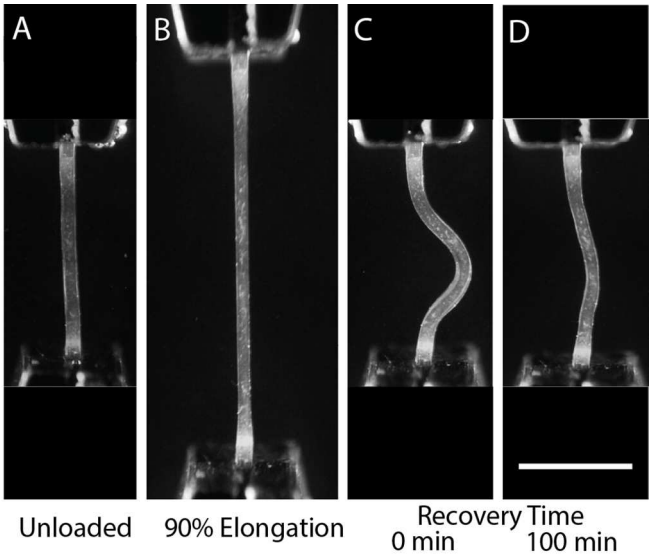

Figure 4. Spontaneous recovery of initial length of a Ca^{2+}-hydrogel strained to 90% underwater.

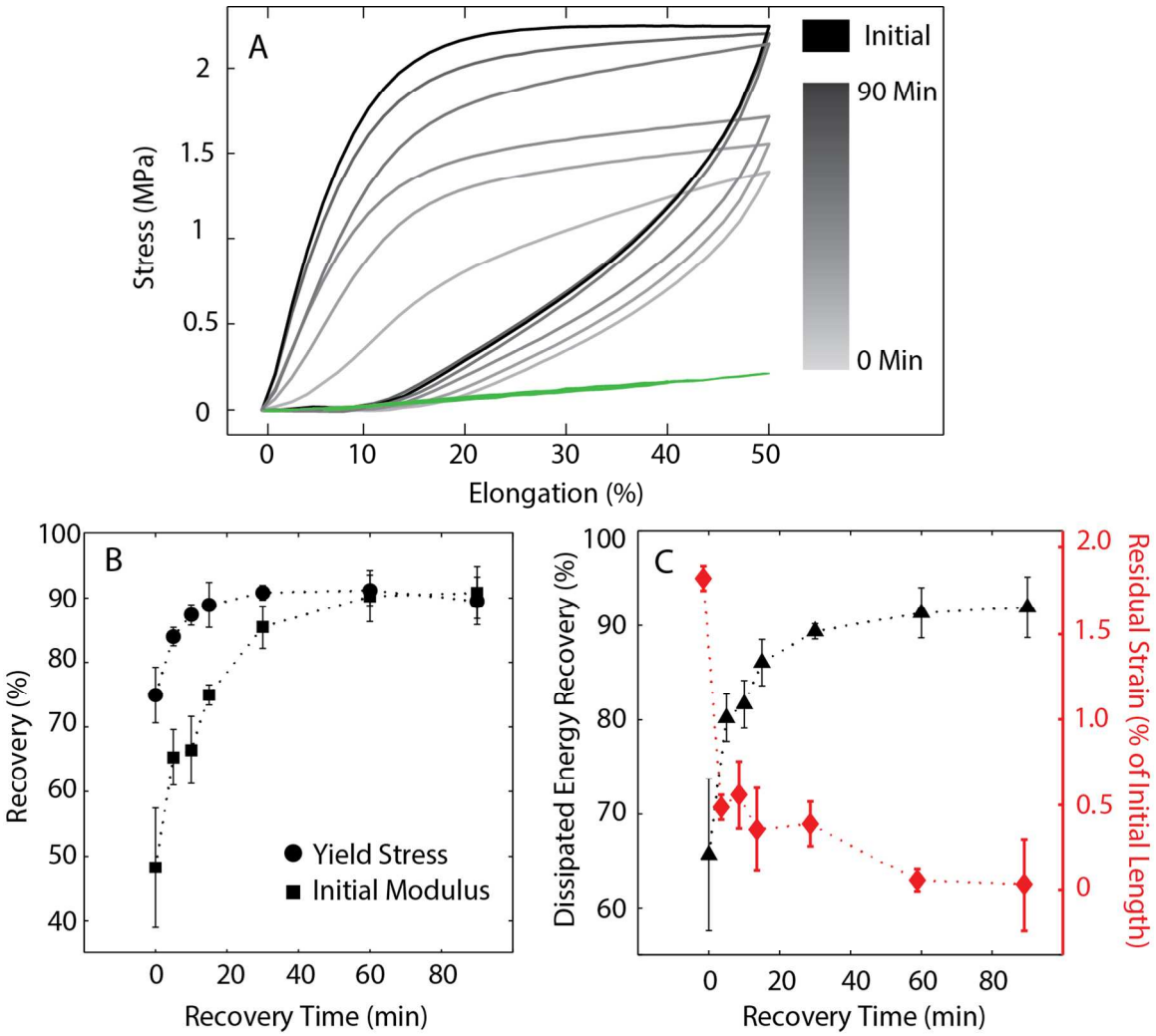

Figure 5. Recovery kinetics of divalent metal ion-equilibrated hydrogels. A) Representative stress strain profiles with increasing recovery periods between cycles. Grey curves: Ca^{2+}. Green curves: Mg^{2+}. B) Time course of initial modulus and yield stress recovery. C) Time course of hysteresis and initial length recovery. Error bars = ± 1 s.d., n ≥ 3.

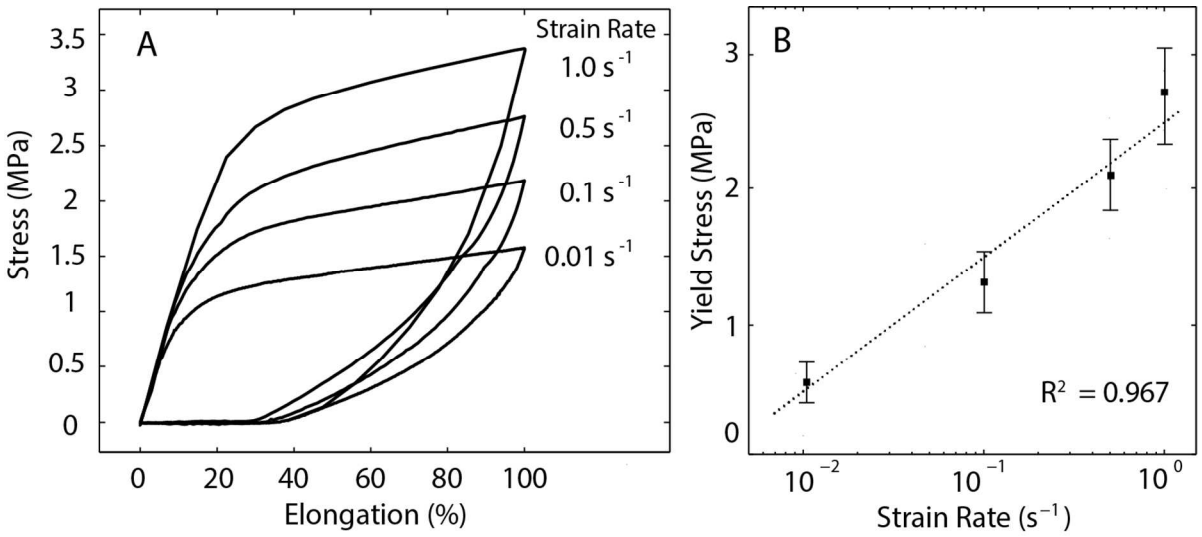

Figure 6. Strain rate dependence of Ca^{2+}-hydrogel stress response. A.) Representative stress strain curves of B.) Semi-log plot of yield stress as a function of strain rate. Dashed lines are best linear fit. Error bars = ± 1 s.d., n ≥ 3.

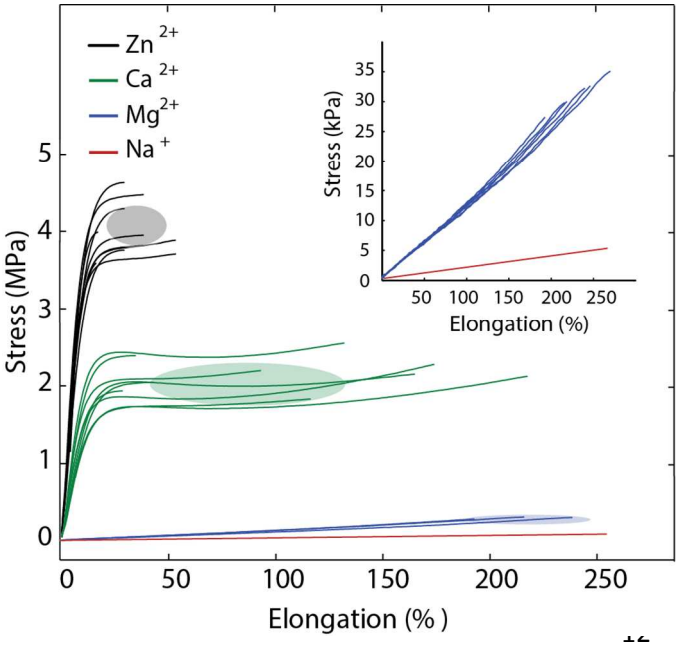

Figure 7. Stress response during strain to fracture for hydrogels equilibrated with Na^{+}, Mg^{2+}, Ca^{2+}, and Zn^{2+}. Ellipses represent the mean ± 1 s.d. Inset: expanded scale to accent Mg^{2+} and Na^{+} hydrogel stress response.

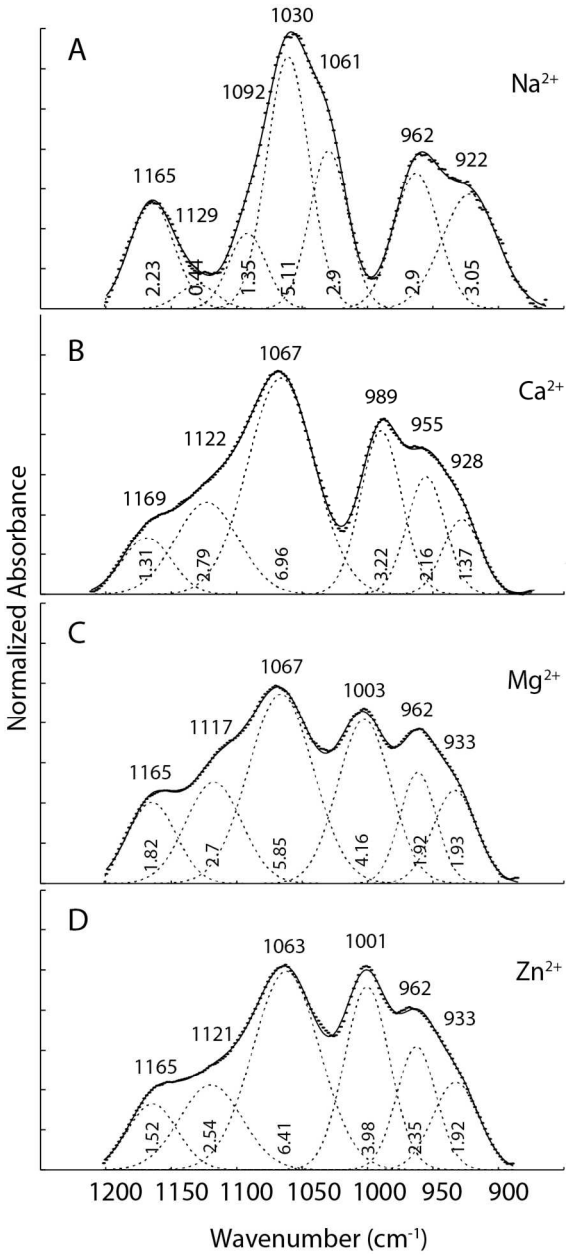

16

17 **Figure 8.** Normalized ATR-FTIR spectra in the region corresponding to P-O^- vibrational modes of

18 metal ion equilibrated hydrogels. A.) Na^+-equilibrated hydrogels. B.) Ca^+-equilibrated

19 hydrogels. C.) Mg^+-equilibrated hydrogels. D.) Zn^+-equilibrated hydrogels. The vertical numbers

20 are the area of the fit peak (dotted spectra) in normalized absorption units.

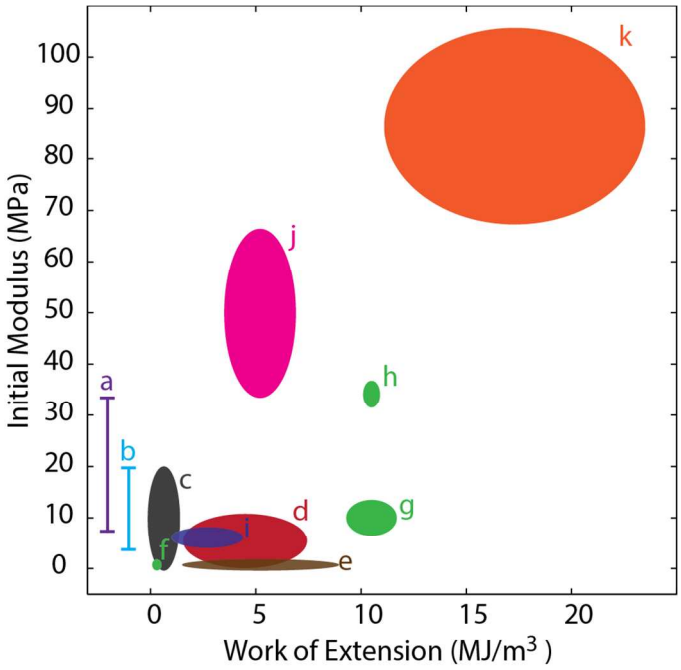

Figure 9. Initial modulus versus toughness for several categories of hydrated materials. Ovals represent the area enclosed by ± 1 s.d. of the initial modulus and work of extension to fracture. a) dipole-dipole,[10] b) PEG/pAAm,[8] c) ionic triblock copolymers,[13] d) polyampholytes,[11] e) highly extensible hydrogels,[7,9,14] f) Mg^{2+}-pMOEP/pAAm,g) Ca^{2+}-pMOEP/pAAm, this report h) Zn^{2+}-pMOEP/pAAm, this report i) articular cartilage,[42] j) meniscus,[42] k) caddisworm silk.[19]

TOC graphic

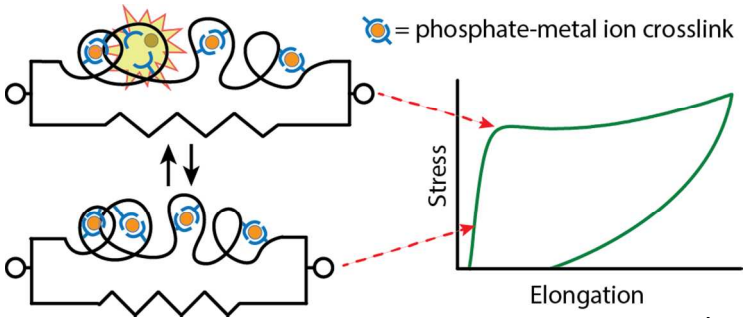

Hydrogels modeled after aquatic caddisworm silk, comprising an elastic polyacrylamide network coupled to a network crosslinked by reversible metal ion-phosphate coordination complexes, display viscoelastic yield behavior and nearly full recovery during cyclical strains.